Efficient Simulation Of The Yaybahar Using A Modal Approach

Conference Paper · September 2023

CITATIONS
0

READS
92

3 authors:

Riccardo Russo
University of Bologna
11 PUBLICATIONS **7** CITATIONS
SEE PROFILE

Michele Ducceschi
University of Bologna
60 PUBLICATIONS **371** CITATIONS
SEE PROFILE

Stefan Bilbao
The University of Edinburgh
221 PUBLICATIONS **3,342** CITATIONS
SEE PROFILE

EFFICIENT SIMULATION OF THE YAYBAHAR USING A MODAL APPROACH

Riccardo Russo, Michele Ducceschi

Department of Industrial Engineering
University of Bologna
Viale Risorgimento 2, Bologna, Italy
riccardo.russo19@unibo.it
michele.ducceschi@unibo.it

Stefan Bilbao

Acoustics & Audio Group
University of Edinburgh
Edinburgh, UK
sbilbao@ed.ac.uk

ABSTRACT

This work presents a physical model of the yaybahar, a recently invented acoustic instrument. Here, output from a bowed string is passed through a long spring, before being amplified and propagated in air via a membrane. The highly dispersive character of the spring is responsible for the typical synthetic tonal quality of this instrument. Building on previous literature, this work presents a modal discretisation of the full system, with fine control over frequency-dependent decay times, modal amplitudes and frequencies, all essential for an accurate simulation of the dispersive characteristics of reverberation. The string-bow-bridge system is also solved in the modal domain, using recently developed non-iterative numerical methods allowing for efficient simulation.

1. INTRODUCTION

The yaybahar is an acoustic musical instrument, recently invented by Turkish artist Görkem Şen [1]. It consists of a neck, with two strings and a fretboard, to which two long springs are attached; each spring is in turn connected, on its opposite end, to a tensioned membrane. The instrument, depicted in Figure 1, is played by either bowing and plucking the strings, or by hitting the springs and the membranes with a mallet. The yaybahar can be described as a cello-like instrument, where amplification is provided by springs and membranes, and not by a resonant body. This structure provides a distinctive reverberant sound, mainly due to the characteristic sound transmission of springs [1]. Given its modular design, the yaybahar lends itself well to physical modeling simulation: in fact, all its components are widely studied systems in physical modeling literature [1, 2, 3]; therefore, a model can be implemented by first simulating the different modules, and by then connecting them together appropriately. A first physical model of the yaybahar was recently proposed by Christensen et al. [4]. There, the strings and membranes are described by the Kirchhoff-Carrier and the Berger models respectively [2, Chapters 8, 13], thus incorporating mild nonlinear effects, while the spring is modeled by a linear stiff bar, following [5]. The components are then coupled by lumped, spring-like connections, and the full model is simulated by using finite-difference-time-domain (FDTD) methods.

[1] https://www.gorkemsen.com/gorkem-sen-s-yaybahar

[2] https://commons.wikimedia.org/wiki/File:Yaybahar.jpg

Figure 1: *The yaybahar (Source [2])*

In this work, a different approach is proposed, based on a modal decomposition of the subsystems. The bowed string, in particular, is simulated in the modal domain following the non-iterative procedure developed in [6], and building on the results presented in [7]. The spring and the membrane, acting as reverberation units, can be simulated efficiently in the modal domain, incorporating refined loss profiles for realistic reverberation [8, 9]. Here, the interconnection between subsystems is performed in an energy-consistent framework via boundary forces, rather than using additional spring-like connections as in [4]. To this end, a novel model for the coupling between a vibrating string and a distributed bridge is presented, in the modal domain, which serves as an emulation for the neck. Given the low amplitude of vibration in the subsystems, linear models for the resonators are adopted without compromising the realism of the sound synthesis overall, as the nonlinear bowing mechanism is largely responsible for the typical drone-like sound of the instrument.

The paper is structured as follows: Section 2 presents the mathematical models of the instrument subcomponents, Section 3 describes the semi-discretisation in the modal domain, Section 4 illustrates the time-stepping algorithms, Section 5 presents the results of a case study and, finally, Section 6 concludes the paper.

2. MODELS

In this section, continuous models for the various components of the yaybahar are presented. A diagram of the instrument's subsystems (bow, string and bridge) and their couplings is as shown in Figure 2. The resulting bridge force is fed to the spring, and the spring sets the membrane into vibration. As shown below,

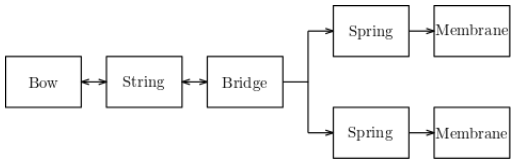

Figure 2: *A scheme of the instrument model and the elements connections.*

the string-bridge coupling modifies significantly the distribution of the eigenfrequencies compared to the isolated string. On the other hand, the spring and the membrane, acting as reverberant units characterised by a large modal density, are less affected by couplings at the boundaries. This justifies their inclusion as non-interacting subsystems, thus considerably simplifying the modal approach. This design shares some similarities with the commuted synthesis approach [10].

For simplicity, in this section, the models are presented here with no damping, except for friction losses induced by the bow. Viscous-type and radiation damping will be introduced in a frequency-dependent manner in the modal domain, as illustrated in Section 3.4.

2.1. Bowed Stiff String and Distributed Bridge

The equations for the coupled bowed string/bridge system are given here as follows:

$$\rho_s \partial_t^2 u_\mathrm{s} = T_\mathrm{s} \partial_x^2 u_\mathrm{s} - \kappa_\mathrm{s}^2 \partial_x^4 u_\mathrm{s} - F_\mathrm{b} \delta(x - x_\mathrm{b}) \phi(\eta), \tag{1a}$$

$$\rho_\mathrm{p} \partial_t^2 u_\mathrm{p} = -\kappa_\mathrm{p}^2 \partial_z^4 u_\mathrm{p} + \delta(z - z_\mathrm{s}) F_\mathrm{s}(t). \tag{1b}$$

Here, subscripts $\mathrm{s}, \mathrm{p}, \mathrm{b}$ refer, respectively, to the string, the bridge ("ponticello") and the bow. In the system above assumes that the string and the bridge vibrate in a single, vertical polarisation, thus neglecting the rocking motion observed in instruments such as the violin [11]. In (1a), $u_\mathrm{s} = u_\mathrm{s}(x,t) : [0, L_\mathrm{s}] \times \mathbb{R}_0^+ \to \mathbb{R}$ represents

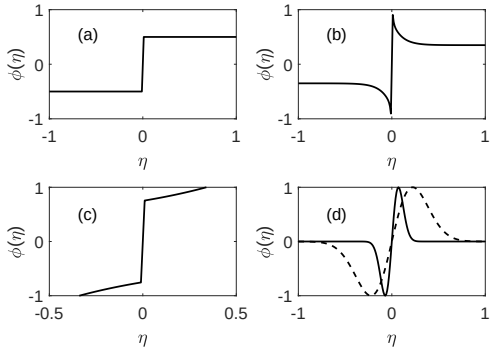

Figure 3: *Some friction characteristics: (a) Coulomb dry friction; (b) the curve by Woodhouse and Smith [12]; (c) the curve by Galluzzo [13]; (d) the continuous curve defined in equation 3, with $a = 10$ (dashed line) and $a = 100$ (solid line). For the mathematical expressions of the four friction characteristics refer to [6].*

the transverse displacement of a string of length L_s in a single polarisation, as a function of spatial coordinate x and time t. ρ_s is the string linear density in kg m^{-1}; T_s is the string tension in N, and κ_s is a rigidity constant in N$^{1/2}$m (κ_s^2 is typically given as the product of Young's modulus times the moment of inertia). Analogous definitions hold for (1b), the equation describing the displacement $u_\mathrm{p} = u_\mathrm{p}(z,t) : [0, L_\mathrm{p}] \times \mathbb{R}_0^+ \to \mathbb{R}$ of the bridge. Here and elsewhere the n$^{\text{th}}$ partial derivative with respect to the variable α is denoted by ∂_α^n.

In (1a), the string is coupled with a bow model, following [6]. The bow excitation is assumed to act pointwise downward at x_b, according to the dimensionless friction coefficient ϕ, as seen in [14]. Various choices for this coefficient are available, see e.g. [12, 13, 2] and also Figure 3. Note that all the four curves displayed in Figure 3 satisfy:

$$\eta\, \phi(\eta) \geq 0, \quad \lim_{|\eta| \to 0} \phi(\eta)/\eta < \infty\,, \tag{2}$$

allowing a non-iterative time stepping procedure to be used, following recent results in [7]. Here, for illustrative purposes, the "soft" characteristic defined in [2] was chosen, defined as:

$$\phi(\eta) = \sqrt{2a}\, \eta\, e^{-a\eta^2 + \frac{1}{2}}\,, \;\; \eta := \partial_t u(x_\mathrm{b}, t) - v_\mathrm{b}. \tag{3}$$

The input bow parameters are the bow force F_b, in N, and the bow velocity v_b in m s^{-1}. Furthermore, in (3), a is a free parameter of the model adjusting the slope of the curve.

The coupling between the string and the bridge takes place at the string's right boundary, and is expressed as an input force F_s in the bridge equation (1b). The string is assumed to be in contact with the bridge at z_s along the bridge's domain. The string's left boundary, as well as the bridge's endpoints, are all assumed to be simply-supported. The complete set of boundary conditions to be imposed is:

$$u_\mathrm{p}(0,t) = \partial_z^2 u_\mathrm{p}(0,t) = u_\mathrm{p}(L_\mathrm{p},t) = \partial_z^2 u_\mathrm{p}(L_\mathrm{p},t) = 0, \tag{4a}$$

$$u_\mathrm{s}(0,t) = \partial_x^2 u_\mathrm{s}(0,t) = \partial_x^2 u_\mathrm{s}(L_\mathrm{s},t) = 0, \tag{4b}$$

$$F_\mathrm{s}(t) = -T_0 \partial_x u_\mathrm{s}(L_\mathrm{s},t) + \kappa_\mathrm{s}^2 \partial_x^3 u_\mathrm{s}(L_\mathrm{s},t), \tag{4c}$$

$$u_\mathrm{p}(z_\mathrm{s},t) = u_\mathrm{s}(L_\mathrm{s},t). \tag{4d}$$

The relations above are assumed to hold $\forall t \geq 0$. Note that (4d) represents a rigid contact condition between the string and the bridge.

2.1.1. Energy Balance

An energy balance for the bridge is obtained after multiplying (1b) by $\partial_t u_\mathrm{p}$ and integrating over $[0, L_\mathrm{p}]$. After integration by parts, and owing to (4a), one obtains:

$$\frac{\mathrm{d}}{\mathrm{d}t} \int_0^{L_\mathrm{p}} \underbrace{\left(\frac{\rho_\mathrm{p}}{2} (\partial_t u_\mathrm{p})^2 + \frac{\kappa_\mathrm{p}^2}{2} (\partial_z^2 u_\mathrm{p})^2 \right)}_{\mathcal{H}_\mathrm{p}} \mathrm{d}z = \dot{u}_\mathrm{p}(z_\mathrm{s},t) F_\mathrm{s}. \tag{5}$$

The string energy balance is obtained analogously, by multiplying equation (1a) by $\partial_t u_\mathrm{s}$ and integrating. After suitable integration by parts, and taking into account the boundary conditions (4b) and (4c), one obtains:

$$\frac{\mathrm{d}}{\mathrm{d}t} \int_0^{L_\mathrm{s}} \underbrace{\left(\frac{\rho_\mathrm{s}}{2} (\partial_t u_\mathrm{s})^2 + \frac{T_\mathrm{s}}{2} (\partial_x u_\mathrm{s})^2 + \frac{\kappa_\mathrm{s}^2}{2} (\partial_x^2 u_\mathrm{s})^2 \right)}_{\mathcal{H}_\mathrm{s}} \mathrm{d}x = $$

$$= -F_\mathrm{s} \dot{u}_\mathrm{s}(L_\mathrm{s},t) - F_\mathrm{b}\, \dot{u}(x_\mathrm{b},t)\, \phi(\dot{u}(x_\mathrm{b},t)). \tag{6}$$

Finally, owing to the contact condition (4d), and by means of (5), one may express (6) as:

$$\frac{\mathrm{d}}{\mathrm{d}t}\left(\int_0^{L_\mathrm{s}} \mathcal{H}_\mathrm{s}\,\mathrm{d}x + \int_0^{L_\mathrm{p}} \mathcal{H}_\mathrm{p}\,\mathrm{d}z\right) = -\mathcal{Q} + \mathcal{P}, \tag{7}$$

where the dissipated and supplied power are defined as, respectively, $\mathcal{Q} := F_\mathrm{b}\,\eta\,\phi(\eta)$, $\mathcal{P} := -F_\mathrm{b}\,v_\mathrm{b}\,\phi(\eta)$. Owing to property (2), in the combined system the energy is non-increasing when the bow velocity v_b (and, therefore, the supplied power $\mathcal{P}$) is identically zero, leading to boundedness of the solutions.

Finally, the output force exerted by the bridge onto the spring is then computed at the desired location z_o as:

$$F_\mathrm{p}(t) = -\kappa_\mathrm{p}^2 \partial_z^3 u_\mathrm{p}(z_\mathrm{o}, t). \tag{8}$$

2.2. Spring

A model of a thin spring that takes into account the helical structure is here implemented, following [3]. In fact, the "bar" model of a spring holds for specific geometries [5], and cuts the low-frequency echoes that are characteristic of spring reverberators [1]. The system is developed starting from Wittrick's equations [15], under the assumption that the wire radius-helix radius ratio r_c/R_c is small [16] (see Figure 4). This allows the model to be reduced to a system of four equations, which relate the displacement in the transverse and longitudinal directions to the moments along the same directions:

$$\mathbf{A}\partial_t^2\mathbf{v} = \mathbf{R}\,\partial_s\mathbf{m} + \delta(s - s_\mathrm{p})\boldsymbol{\alpha}_\mathrm{p}F_\mathrm{p}, \quad \mathbf{D}\mathbf{m} = \mathbf{R}\partial_s\mathbf{v}. \tag{9}$$

Here, $\mathbf{v} := [v_\tau(s,t), v_\lambda(s,t)]^\intercal : [0, L_c] \times \mathbb{R}_0^+ \to \mathbb{R}^2$ is the vector of displacements, where the subscripts τ and λ refer to the transverse and longitudinal directions, respectively. Analogously, $\mathbf{m} := [m_\tau, m_\lambda]^\intercal$ is the vector of moments. Above, s expresses the arclength of the coil, such that $0 \leq s \leq L_c$. The input force F_p, computed in equation (8), is applied pointwise at $s = s_\mathrm{p}$, while the vector $\boldsymbol{\alpha}_\mathrm{p}$ is a unit vector that indicates the amount of force exerted in both polarisations. The matrices $\mathbf{A}, \mathbf{D} \in \mathbb{R}^{2\times2}$ are diagonal, and given by:

$$\mathbf{A} = \rho_\mathrm{c}\begin{bmatrix}1 & 0\\ 0 & 1 - l^2\partial_s^2\end{bmatrix}, \quad \mathbf{D} = \kappa_c^{-2}\begin{bmatrix}1 & 0\\ 0 & 1 + \nu_c - l^2\partial_s^2\end{bmatrix}. \tag{10}$$

Above, ρ_c is the linear density of the coil, in kg m^{-1}, κ_c is a rigidity constant in N$^{1/2}$m, and ν_c is the Poisson ratio of the coil. $\mathbf{R} \in \mathbb{R}^{2\times2}$ is a symmetric matrix, of the form:

$$\mathbf{R} = \begin{bmatrix}-2\mu/l & (1-\mu^2)/l + l\partial_s^2\\ 0 & 2\mu(l\partial_s^2 + 1/l)\end{bmatrix}. \tag{11}$$

The symbol l denotes the ratio $R_c/\cos^2(\theta)$, where θ is the pitch angle, R_c the coil radius, and μ is shorthand for $\tan(\theta)$. A graphical representation of the spring physical quantities is provided in Figure 4.

2.2.1. Energy Analysis

The energy balance and boundary conditions may be obtained, in the zero-input ($F_\mathrm{p} = 0$) case, as follows. First, left-multiply the first equation in (9) by $\partial_t\mathbf{v}^\intercal$. Then, take a time derivative of the second equation in (9), and left-multiply by $\mathbf{m}^\intercal$, where $\intercal$ is the transposition operator. Integrating the resulting equations gives:

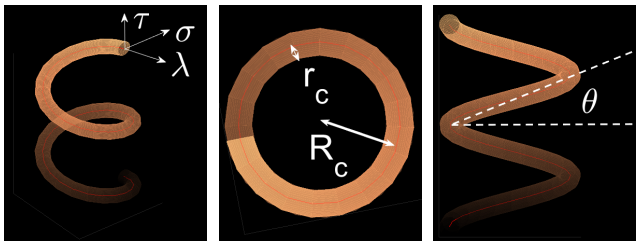

(a) *Directions.* (b) *Wire/helix radius.* (c) *Tilt angle.*

Figure 4: *Spring physical quantities.*

$$\int_0^{L_c} \partial_t\mathbf{v}^\intercal\mathbf{A}\,\partial_t^2\mathbf{v}\,\mathrm{d}s = \int_0^{L_c} \partial_t\mathbf{v}^\intercal\mathbf{R}\,\partial_s\mathbf{m}\,\mathrm{d}s, \tag{12a}$$

$$\int_0^{L_c} \mathbf{m}^\intercal\mathbf{D}\,\partial_t\mathbf{m}\,\mathrm{d}s = \int_0^{L_c} \mathbf{m}^\intercal\mathbf{R}(\partial_s\partial_t\mathbf{v})\,\mathrm{d}s. \tag{12b}$$

Integrating by parts to the right-hand side of (12b), one is able to express the right-hand side of (12a), which, in turn, can be rewritten as:

$$\int_0^{L_c} \left(\partial_t\mathbf{v}^\intercal\mathbf{A}\,\partial_t^2\mathbf{v} + \mathbf{m}^\intercal\mathbf{D}\,\partial_t\mathbf{m}\right)\mathrm{d}s = \left(\mathcal{B}_0 + \mathbf{m}^\intercal\mathbf{R}\,\partial_t\mathbf{v}\right)\big|_0^{L_c}.$$

Here

$$\mathcal{B}_0 := l\partial_s\partial_t v_\lambda\left(\partial_s m_\tau + 2\mu\partial_s m_\lambda\right) + \partial_t v_\lambda(2\mu l\partial_s^2 m_\lambda - l\partial_s^2 m_\tau) - l\partial_s\partial_t v_\tau(\partial_s m_\lambda) - \partial_t v_\tau(l\partial_s^2 m_\lambda). \tag{13}$$

By further applying integration by parts, one derives the energy balance:

$$\frac{\mathrm{d}}{\mathrm{d}t}\int_0^{L_c} \mathcal{H}_\mathrm{c}\,\mathrm{d}s = \left(\mathcal{B}_0 + \mathcal{B}_1 + \mathbf{m}^\intercal\mathbf{R}\,\partial_t\mathbf{v}\right)\big|_0^{L_c} := \mathcal{B}_\mathrm{c}\big|_0^{L_c}. \tag{14}$$

Here, the energy density is:

$$\mathcal{H}_\mathrm{c} = \frac{\rho_\mathrm{c}}{2}\left((\partial_t v_\tau)^2 + (\partial_t v_\lambda)^2 + l^2(\partial_t\partial_s v_\lambda)^2\right) + \frac{\kappa_\mathrm{c}^{-2}}{2}\left(m_\tau^2 + (1+\nu_\mathrm{c})m_\lambda^2 + l^2(\partial_s m_\lambda)^2\right); \tag{15}$$

while $\mathcal{B}_1$ is:

$$\mathcal{B}_1 = l^2\rho_\mathrm{c}(\partial_t v_\lambda)(\partial_s\partial_t^2 v_\lambda) + l^2\kappa_\mathrm{c}^{-2}m_\lambda(\partial_s\partial_t m_\lambda). \tag{16}$$

It is useful to write the boundary terms in terms of the conjugate variables forces / velocities and moments / angular velocities [3]. To that end, rearranging the boundary terms in (14) allows to write:

$$\mathcal{B}_\mathrm{c} = F_\tau\partial_t v_\tau + F_\lambda\partial_t v_\lambda + F_\sigma\partial_t v_\sigma + m_\tau\phi_\tau + m_\lambda\phi_\lambda + m_\sigma\phi_\sigma.$$

Here, the σ denotes the direction perpendicular to the (τ, λ)-plane. Denoting $g := -\frac{\mu^2}{l} + \frac{1}{l} + l\partial_s^2$, one has

$$F_\tau = g\, m_\lambda - 2\mu m_\tau / l, \tag{17a}$$
$$F_\lambda = g\, m_\tau + 2\mu \left(l\partial_s^2 + 1/l\right) m_\lambda + l^2 \rho_\mathrm{c} \partial_s \partial_t^2 v_\lambda, \tag{17b}$$
$$F_\sigma = -\partial_s (m_\tau + 2\mu m_\lambda), \tag{17c}$$
$$\phi_\tau = l\partial_s^2 \partial_t v_\lambda, \tag{17d}$$
$$\phi_\lambda = 2\mu l \partial_s^2 \partial_t v_\lambda + l^2 \kappa_\mathrm{c}^{-2} \partial_s \partial_t m_\lambda + l\partial_s^2 \partial_t v_\tau, \tag{17e}$$
$$\phi_\sigma = -\partial_s \partial_t v_\tau, \tag{17f}$$
$$m_\sigma = l\partial_s m_\lambda, \tag{17g}$$
$$v_\sigma = l\partial_s v_\lambda. \tag{17h}$$

Setting boundary displacements, forces and moments to zero leads to a generalisation of the classic beam boundary conditions of free, simply-supported or clamped type. Here, a variant of free boundary conditions along τ, λ will be used, combined with clamped conditions along σ. Hence:

$$F_\tau = F_\lambda = m_\tau = m_\lambda = v_\sigma = \phi_\sigma = 0. \tag{18}$$

These are intended to hold at the boundary points $s = \{0, L_\mathrm{c}\}$, and $\forall t \geq 0$. An output signal $F_\mathrm{c}(t)$ may be then be extracted by computing the sum of the forces F_τ, F_λ, F_σ at a s_o, close, but not equal, to the boundary L_c. Thus:

$$F_\mathrm{c}(t) = F_\tau(s_\mathrm{o}, t) + F_\lambda(s_\mathrm{o}, t) + F_\sigma(s_\mathrm{o}, t). \tag{19}$$

2.3. Membrane

A model for the membrane is given by the 2D wave equation [2, Chapter 11]:

$$\rho_m \partial_t^2 w = T_m \nabla^2 w + \delta(X - X_\mathrm{c})\delta(Y - Y_\mathrm{c}) F_\mathrm{c}(t). \tag{20}$$

In the above, the two dimensional Laplacian was introduced as $\nabla^2 := \partial_X^2 + \partial_Y^2$. For simplicity, and to avoid the introduction of further symbols, the membrane is supposed to be defined over a square, of side length L_m. Thus, $w = w(X, Y, t) : [0, L_m] \times [0, L_m] \times \mathbb{R}^+ \to \mathbb{R}$ describes the displacement of the membrane in the transversal direction, ρ_m is the material surface density in kg m^{-2}, and T_m is the tension applied at the edges in N m^{-1}. An energy analysis for this system can be found in [2, Chapter 11]. Boundary conditions of fixed type will be considered here, such that:

$$w(0, Y) = w(L_m, Y) = w(X, 0) = w(X, L_m) = 0. \tag{21}$$

3. SEMI-DISCRETISATION

The equations presented in Section 2 will be now semi-discretised in space using a modal approach. While the spring and the membrane possess an analytical form for the modes of vibration, this is not true in the case of a string coupled with a distributed bridge on one end. For this reason, the modal expansion for the latter system will be performed by solving the eigenvalue problem numerically.

3.1. Bowed Stiff String and Distributed Bridge

First, it is convenient to introduce spatial difference operators. The string domain is divided into M_s subintervals of length h, the grid spacing. This yields $M_\mathrm{s} + 1$ discretisation points, including the end points. Analogously, the bridge is divided into M_p subintervals of length h. The continuous functions $u_\mathrm{s}(x, t)$ and $u_\mathrm{p}(z, t)$ are then approximated by grid functions $u_\mathrm{s}^m(t) \approx u_\mathrm{s}(mh, t)$ and $u_\mathrm{p}^n(t) \approx u_\mathrm{p}(nh, t)$, for integer m, n. In light of the numerical boundary conditions given below, one has $m \in [1, ..., M_\mathrm{s} - 1]$, $n \in [1, ..., M_\mathrm{p} - 1]$. In vector notation, the grid functions will be denoted $\mathbf{u}_\mathrm{s}$, $\mathbf{u}_\mathrm{p}$.

Basic forward and backward difference operators, approximating the first spatial derivative, and acting on u_s^m, are:

$$\delta_x^\pm u_\mathrm{s}^m = \pm(u_\mathrm{s}^{m\pm1} - u_\mathrm{s}^m)/h. \tag{22}$$

Analogous definitions hold for the grid function u_p^n, thus, for instance, $\delta_z^+ u_\mathrm{p}^n = (u_\mathrm{p}^{n+1} - u_\mathrm{p}^n)/h$. The second and fourth spatial derivatives are approximated by difference operators obtained by combining the operators above, as:

$$\delta_x^2 := \delta_x^+ \delta_x^-, \qquad \delta_x^4 := \delta_x^2 \delta_x^2, \tag{23}$$

with similar definitions holding for δ_z^2, δ_z^4. Discrete versions of the Dirac deltas in (1) are also needed. To that end, $\delta(x - x_\mathrm{b})$ in (1a) is approximated by the column vector $\mathbf{d}_\mathrm{b}$, of length $M_\mathrm{s} - 1$, as:

$$d_\mathrm{b}^\nu = (1 - \alpha)/h, \qquad d_\mathrm{b}^{\nu+1} = \alpha/h, \tag{24}$$

where $\nu := \mathrm{floor}(x_\mathrm{b}/h)$, $\alpha := x_\mathrm{b}/h - \nu$. An analogous definition holds for $\mathbf{d}_\mathrm{s}$, approximating $\delta(z - z_\mathrm{s})$ in (1b).

3.1.1. Semi-Discrete Formulation

Given the definitions above, a semi-discrete approximation of (1) is given as:

$$\rho_\mathrm{s} \ddot{u}_\mathrm{s}^m = T_\mathrm{s} \delta_x^2 u_\mathrm{s}^m - \kappa_\mathrm{s}^2 \delta_x^4 u_\mathrm{s}^m - F_\mathrm{b} d_\mathrm{b}^m \phi(\eta), \tag{25a}$$
$$\rho_\mathrm{p} \ddot{u}_\mathrm{p}^n = -\kappa_\mathrm{b}^2 \delta_z^4 u_\mathrm{p}^n + d_\mathrm{s}^n f_\mathrm{s}(t). \tag{25b}$$

Here, $\eta = h\mathbf{d}_\mathrm{b}^\intercal \dot{\mathbf{u}}_\mathrm{s} - v_\mathrm{b}$. A discrete version of the boundary conditions and contact condition (4) ensuring numerical stability is:

$$u_\mathrm{p}^0 = \delta_z^2 u_\mathrm{p}^0 = u_\mathrm{p}^{M_\mathrm{p}} = \delta_z^2 u_\mathrm{p}^{M_\mathrm{p}} = 0, \tag{26a}$$
$$u_\mathrm{s}^0 = \delta_x^2 u_\mathrm{s}^0 = \delta_x^2 u_\mathrm{s}^{M_\mathrm{s}} = 0, \tag{26b}$$
$$f_\mathrm{s}(t) = -T_\mathrm{s} \delta_x^+ u_\mathrm{s}^{M_\mathrm{s}} + \kappa_\mathrm{s}^2 \delta_x^+ \delta_x^2 u_\mathrm{s}^{M_\mathrm{s}}, \tag{26c}$$
$$h\mathbf{d}_\mathrm{s}^\intercal \mathbf{u}_\mathrm{p} = u_\mathrm{s}^{M_\mathrm{s}}. \tag{26d}$$

By expanding the operators and applying the boundary conditions, the semi-discrete equations can be arranged in vector form. To that end, define $\mathbf{u}^\intercal := [\mathbf{u}_\mathrm{s}^\intercal, \mathbf{u}_\mathrm{p}^\intercal]$. System (25) can be then written in compact form as:

$$\mathbf{M}\ddot{\mathbf{u}} = -\mathbf{K}\mathbf{u} - F_\mathrm{b} \mathbf{J}_\mathrm{b} \phi(\eta). \tag{27}$$

Here, $\mathbf{J}_\mathrm{b}$ is a vector obtained by concatenating $\mathbf{d}_\mathrm{b}$ with a zero-vector of dimension M_{p-1}, and $\eta = h\mathbf{J}_\mathrm{b}^\intercal \dot{\mathbf{u}} - v_\mathrm{b}$. $\mathbf{M}$ is positive-definite, symmetric, square diagonal block matrix, with diagonal blocks given as:

$$\mathbf{M}_{11} = \rho_\mathrm{s} \mathbf{I}_\mathrm{s}, \ \mathbf{M}_{22} = \left(\rho_\mathrm{p} \mathbf{I}_\mathrm{p} + \rho_\mathrm{s} h^2 \mathbf{d}_\mathrm{s} \mathbf{d}_\mathrm{s}^\intercal\right). \tag{28}$$

Here, $\mathbf{I}_\mathrm{s}$ and $\mathbf{I}_\mathrm{p}$ are identity matrices, of dimension $(M_\mathrm{s} - 1) \times (M_\mathrm{p} - 1)$ and $(M_\mathrm{p} - 1) \times (M_\mathrm{s} - 1)$ respectively. Furthermore,

the stiffness matrix is a positive-definite, square block matrix, with blocks:

$$\begin{aligned}\mathbf{K}_{11} &= -T_\mathrm{s}\mathbf{D}_x^2 + \kappa_\mathrm{s}^2\mathbf{D}_x^2\mathbf{D}_x^2,\\ \mathbf{K}_{12} &= \mathbf{K}_{21}^\intercal \quad \mathbf{K}_{21} = \left[\mathbf{0}, \tfrac{\kappa_\mathrm{s}^2}{h^3}\mathbf{d}_\mathrm{s}, -\left(\tfrac{T_\mathrm{s}}{h^2} + \tfrac{2\kappa_\mathrm{s}^2}{h^3}\right)\mathbf{d}_\mathrm{s}\right],\\ \mathbf{K}_{22} &= \kappa_\mathrm{p}^2\mathbf{D}_z^2\mathbf{D}_z^2 + \left(T_\mathrm{s} + \frac{2\kappa_\mathrm{s}^2}{h^2}\right)\mathbf{d}_\mathrm{s}\mathbf{d}_\mathrm{s}^\intercal,\end{aligned} \tag{29}$$

where $\mathbf{D}_x^2$ and $\mathbf{D}_z^2$ are the second difference operators with Dirichlet end conditions of dimensions, respectively, $(M_\mathrm{s}-1)\times(M_\mathrm{s}-1)$, and $(M_\mathrm{p}-1)\times(M_\mathrm{p}-1)$ (for the explicit form of these matrices, see [2, Chapter 5]). $\mathbf{K}_{21}$ has dimension $(M_\mathrm{p}-1)\times(M_\mathrm{s}-1)$, and is a composition of a zero-matrix of dimension $(M_\mathrm{p}-1)\times(M_\mathrm{s}-3)$ with two vectors.

An energy balance in the modal domain is readily available from (27), after left-multiplying by $h\dot{\mathbf{u}}^\intercal$. When $v_\mathrm{b}=0$, one has:

$$\frac{\mathrm{d}}{\mathrm{d}t}\left(\frac{h}{2}\dot{\mathbf{u}}^\intercal\mathbf{M}\dot{\mathbf{u}} + \frac{h}{2}\mathbf{u}^\intercal\mathbf{K}\mathbf{u}\right) = -\eta\phi(\eta) \leq 0. \tag{30}$$

Since both $\mathbf{M}$, $\mathbf{K}$ are non-negative, the energy is non-negative, and decays over time.

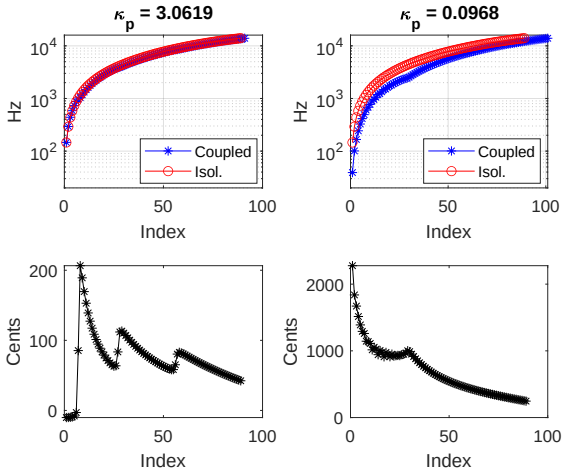

Figure 5: *Eigenfrequencies of the coupled system and the ones of a simply supported stiff string in isolation, under two different values of κ_p. The left value is typical of steel, while the right one was chosen arbitrarily low for demonstration purposes. Other physical parameters, on common between the two cases, were: $L_\mathrm{s}=0.69$ m; $T_\mathrm{s}=147.7$ N; $\rho_\mathrm{s}=0.0063$ Kg m^{-1}; $\kappa_\mathrm{s}=0.4835$ N$^{1/2}$ m; $L_\mathrm{p}=0.07$ m; $\rho_\mathrm{p}=0.0251$ Kg m^{-1}. The contact point was set to: $z_\mathrm{s}=0.03$ m. The top figures report the frequencies in log scale, while the bottom figures display the difference in cents between frequencies with the same index.*

3.1.2. Modal Expansion

A modal expansion of system (27) is now performed by solving the generalised eigenvalue problem. For that, consider the following:

$$\mathbf{K}\mathbf{U} = \mathbf{M}\mathbf{U}\boldsymbol{\Omega}_\mathrm{u}^2. \tag{31}$$

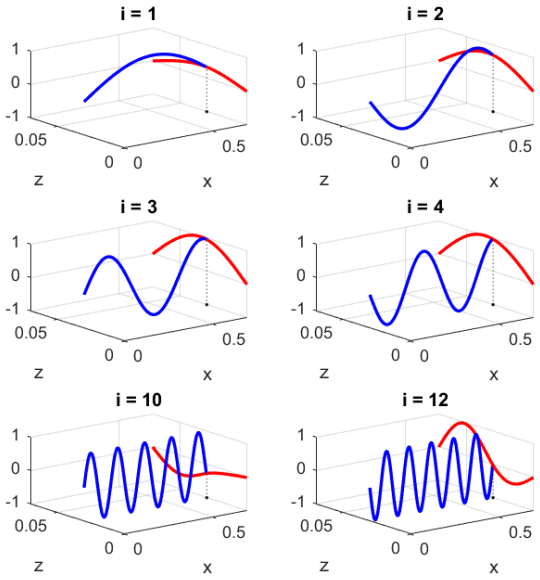

Figure 6: *Modes of the coupled string-bridge system, which were normalized, and plotted orthogonal one to another for visualisation purposes. The letter i gives the mode index. The blue line represents the string, and red one the bridge, while the projection of the contact point on the z-axis is highlighted with a black dot. The physical parameters were the same listed in Figure 5, with $\kappa_\mathrm{p}=3.0619$ N$^{1/2}$ m.*

Here, $\mathbf{U}$ is a matrix of real eigenvectors, and $\boldsymbol{\Omega}^2$ is a diagonal matrix of real, positive eigenvalues. Note that, while both $\mathbf{K}$ and $\mathbf{M}$ are symmetric, the product $\mathbf{M}^{-1}\mathbf{K}$ generally will not be. However, since $\mathbf{M}$ is positive definite, the eigenvalues are then real [17], and they must also be non-negative since so are the eigenvalues of $\mathbf{K}$. Then, define $\mathrm{u}=\mathbf{U}^{-1}\mathbf{u}$. System (27) may then be written as:

$$\ddot{\mathrm{u}} = -\boldsymbol{\Omega}_\mathrm{u}^2\mathrm{u} - F_\mathrm{b}\boldsymbol{\xi}_\mathrm{b}\phi(\eta), \quad \eta = \boldsymbol{\xi}_\eta^\intercal\dot{\mathrm{u}} - v_\mathrm{b}, \tag{32}$$

with $\boldsymbol{\xi}_\eta^\intercal := h\mathbf{J}_\mathrm{b}^\intercal\mathbf{U}$, $\boldsymbol{\xi}_\mathrm{b} := (\mathbf{M}\mathbf{U})^{-1}\mathbf{J}_\mathrm{b}$. This a modal system with a diagonal linear part, with modal coordinates u. One may of course solve the numerical eigenvalue problem (31) using a very fine grid (i.e., using a small grid spacing h), though only a number N_u is kept in (32), fixed by Nyquist requirements.

Before proceeding, it is useful to compare the eigenfrequencies of the string in isolation against those of the coupled string-bridge system. Figure 5 shows two such comparisons, under two different values of κ_p. These are computed for a bar of circular cross section, with a diameter of 5 mm. The first value ($\kappa_\mathrm{p}\approx 3$) is typical of steel, while the second value ($\kappa_\mathrm{c}\approx 0.1$) was selected to artificially amplify the effects of the coupling. The top panels report the frequencies in a log scale: it is seen that the reduced stiffness shifts the eigenfrequencies downwards by up to two octaves in the lowest range, as seen in the bottom panels. With sufficiently large values of κ_p, as is the case of steel, the frequency gap remains contained around the fundamental, as expected, but it increases up to two semitones for larger modal indices. These results underline the importance of considering the string-bridge coupling for in the distribution of the eigenfrequencies.

The eigenmodes are represented in Figure 6, for a steel bridge. Here, the first four modes are displayed, along with the 10th and the 12th. It is possible to see that the bridge eigenmodes start exhibiting a third node only after the 10th mode.

3.2. Spring

A modal version of the thin spring model was originally proposed by van Walstijn [18]. In van Walstijn's model, the modal expansion is carried out numerically, by first performing a semi-discretisation in space, and then computing the eigenvalues of the resulting matrix. Such model found practical application in [19], where a virtual analogue simulation of a spring reverb is developed. In this work an analytic form for the modes is available under a choice of the boundary conditions as per (18). To that end, consider the following:

$$\begin{aligned} \mathbf{v}(s,t) &= \sqrt{2/L_\mathrm{c}}\cos(\gamma s)\,\bar{\mathbf{v}}(t), \\ \mathbf{m}(s,t) &= \sqrt{2/L_\mathrm{c}}\sin(\gamma s)\,\bar{\mathbf{m}}(t), \end{aligned} \tag{33}$$

where $\bar{\mathbf{v}}$, $\bar{\mathbf{m}}$ are the time modal coordinates, and the factor $\sqrt{2/L_\mathrm{c}}$ is just a useful normalisation constant. It is immediate to see that these satisfy the boundary conditions (18) when $\gamma = \{\pi/L_\mathrm{c}, 2\pi/L_\mathrm{c}, ..., n\pi/L_\mathrm{c}, ...\}$.

Let now $\gamma_n := n\pi/L_\mathrm{c}$, for integer n. A solution to the equation of motion is obtained using the quantised expressions of the modes to solve an eigenvalue problem. Left-multiplying the first equation in (9) by $\sqrt{2/L_\mathrm{c}}\cos(\gamma_n s)$, and the second by $\sqrt{2/L_\mathrm{c}}\sin(\gamma_n s)$ and integrating, one is able to express (9) as:

$$\bar{\mathbf{A}}\ddot{\bar{\mathbf{v}}} = \gamma_n\bar{\mathbf{R}}\bar{\mathbf{m}} + \sqrt{2/L_\mathrm{c}}\cos(\gamma_n s_\mathrm{p})\boldsymbol{\alpha}_\mathrm{p}F_\mathrm{p}(t), \tag{34a}$$

$$\bar{\mathbf{D}}\bar{\mathbf{m}} = -\gamma_n\bar{\mathbf{R}}\bar{\mathbf{v}}. \tag{34b}$$

Here, the transformed matrices are obtained by applying the derivatives to the modal functions, and have the form (10), (11) under the replacement of ∂_s^2 by $-\gamma_n^2$. Then, (34b) is used to express $\bar{\mathbf{m}}$ is terms of $\bar{\mathbf{v}}$, and this is substituted in (34a). One gets:

$$\ddot{\bar{\mathbf{v}}} = -\mathbf{V}\boldsymbol{\Omega}_n^2\mathbf{V}^{-1}\bar{\mathbf{v}} + \sqrt{2/L_\mathrm{c}}\cos(\gamma_n s_\mathrm{p})\bar{\mathbf{A}}^{-1}\boldsymbol{\alpha}_\mathrm{p}F_\mathrm{p}.$$

where it was set:

$$\mathbf{V}\boldsymbol{\Omega}_n^2\mathbf{V}^{-1} := \gamma_n^2\bar{\mathbf{A}}^{-1}\bar{\mathbf{R}}\bar{\mathbf{D}}^{-1}\bar{\mathbf{R}}. \tag{35}$$

Here $\mathbf{V}$ is a 2×2 matrix of eigenvectors for the wavenumber γ_n, and $\boldsymbol{\Omega}_n$ is a diagnoal 2×2 matrix of eigenfrequencies. Figure 7 reports the solution to the eigenvalue problem for a typical spring. The eigenfrequencies lay on the yellow an purple lines.

Then, define $\mathfrak{v}_n := (\mathbf{V})^{-1}\bar{\mathbf{v}}$. Thus, one gets:

$$\ddot{\mathfrak{v}}_n = -\boldsymbol{\Omega}_n^2\mathfrak{v} + \sqrt{2/L_\mathrm{c}}\cos(\gamma_n s_\mathrm{p})(\bar{\mathbf{A}}\mathbf{V})^{-1}\boldsymbol{\alpha}_\mathrm{p}F_\mathrm{p}(t). \tag{36}$$

Assume now $n = 1, ..., N_\mathfrak{v}$. The modal equations for the spring are then a system of $2N_\mathfrak{v}$ equations, of the form:

$$\ddot{\mathfrak{v}} = -\boldsymbol{\Omega}_\mathfrak{v}^2\mathfrak{v} + \boldsymbol{\xi}_\mathrm{p}F_\mathrm{p}(t), \tag{37}$$

where $\mathfrak{v}$ is a vector of length $2N_\mathfrak{v}$, $\boldsymbol{\Omega}_\mathfrak{v}$ is a $2N_\mathfrak{v}\times 2N_\mathfrak{v}$ diagonal matrix, whose diagonal elements are the 2×2 diagonal blocks $\boldsymbol{\Omega}_n$, $n = 1, ...N_\mathfrak{v}$ defined in (35), and $\boldsymbol{\xi}_\mathrm{p}$ is a $2N_\mathfrak{v}$ vector made composed by stacking the 2×1 blocks: $\sqrt{2/L_\mathrm{c}}\cos(\gamma_n s_\mathrm{p})(\bar{\mathbf{A}}\mathbf{V})^{-1}\boldsymbol{\alpha}_\mathrm{p}$, $n = 1, ..., N_\mathfrak{v}$.

Output (19) is extracted by substituting the solution (33) into the boundary forces (17c) (17b) and (17a) computed at a position close to L_c.

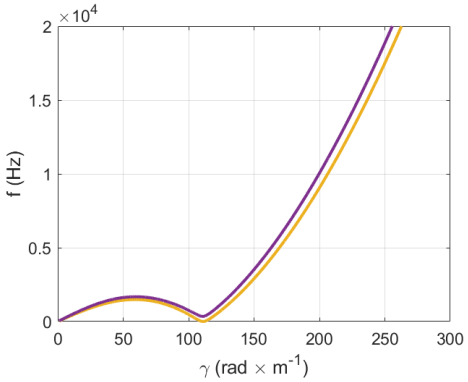

Figure 7: *Plot of the dispersion relation of a thin spring. Physical parameters were chosen to be coherent with a possible yaybahar spring:* $R_\mathrm{c} = 9$ mm, $r_\mathrm{c} = 1$ mm, $\theta = 2°$, $L_\mathrm{c} = 40$ m, $\kappa_\mathrm{c} = 9.9$ *and* $\nu_\mathrm{c} = 0.3$. *These values yield* $N_\mathfrak{v} = 2812$ *within the hearing range.*

3.3. Membrane

A particular solution to equation (20) with fixed boundary conditions (21) is given by:

$$w(X,Y,t) = \frac{2}{L_m}\sin\frac{\beta_X^j\pi X}{L_m}\sin\frac{\beta_Y^j\pi Y}{L_m}\mathfrak{w}_j(t), \tag{38}$$

for integers β_X^j, β_Y^j [20]. The associated modal frequency is:

$$\omega_j = \frac{\pi}{L_m}\sqrt{\frac{T_m}{\rho_m}\left((\beta_X^j)^2 + (\beta_Y^j)^2\right)}. \tag{39}$$

The modal system for the membrane is then given by:

$$\ddot{\mathfrak{w}} = -\boldsymbol{\Omega}_\mathfrak{w}^2\mathfrak{w} + \boldsymbol{\xi}_c F_c(t), \tag{40}$$

where $\mathfrak{w}$ is a $N_\mathfrak{w}\times 1$ vector, $\boldsymbol{\Omega}_\mathfrak{w}$ is a $N_\mathfrak{w}\times N_\mathfrak{w}$ diagonal matrix where the jth diagonal element is ω_j given above. The frequencies should here be sorted in ascending order, such that $\omega_{j-1} \leq \omega_j \leq \omega_{j+1}$, $j = 2, ..., N_\mathfrak{w} - 1$. This allows to find the corresponding modal indices β_X^j, β_Y^j. Above, $\boldsymbol{\xi}_c$ is a $N_\mathfrak{w}\times 1$ vector whose jth component is $\frac{2}{L_m\rho_m}\sin\frac{\beta_X^j\pi X_c}{L_m}\sin\frac{\beta_Y^j\pi Y_c}{L_m}$.

Output is extracted as:

$$w_\mathrm{o}(t) = \sum_{j=1}^{N_\mathfrak{w}}\frac{2}{L_m}\sin\frac{\beta_X^j\pi X_\mathrm{o}}{L_m}\sin\frac{\beta_Y^j\pi Y_\mathrm{o}}{L_m}\mathfrak{w}_j(t), \tag{41}$$

though for synthesis purposes it may be convenient to use $\dot{w}_\mathrm{o}(t)$ instead.

3.4. Modal Equations of the Full System with Loss

The full system in the modal domain can thus be written as an augmented version of (32), (37) and (40). This is:

$$\ddot{\mathfrak{u}}(t) = -\boldsymbol{\Omega}_\mathfrak{u}^2\mathfrak{u}(t) - \mathbf{C}_\mathfrak{u}\dot{\mathfrak{u}}(t) - \boldsymbol{\xi}_\mathrm{b}F_\mathrm{b}\phi(\eta), \tag{42a}$$

$$\ddot{\mathfrak{v}}(t) = -\boldsymbol{\Omega}_\mathfrak{v}^2\mathfrak{v}(t) - \mathbf{C}_\mathfrak{v}\dot{\mathfrak{v}}(t) + \boldsymbol{\xi}_\mathrm{p}F_\mathrm{p}(t), \tag{42b}$$

$$\ddot{\mathfrak{w}}(t) = -\boldsymbol{\Omega}_\mathfrak{w}^2\mathfrak{w}(t) - \mathbf{C}_\mathfrak{w}\dot{\mathfrak{w}}(t) + \boldsymbol{\xi}_c F_c(t), \tag{42c}$$

where $\mathbf{C}_\mathfrak{u}$, $\mathbf{C}_\mathfrak{v}$, $\mathbf{C}_\mathfrak{w}$ are, respectively, $N_\mathfrak{u} \times N_\mathfrak{u}$, $2N_\mathfrak{v} \times 2N_\mathfrak{v}$, $N_\mathfrak{w} \times N_\mathfrak{w}$ positive, diagonal matrices containing the modal loss coefficients in s^{-1}. System (42) depends on time only, and a suitable time stepping routine is offered below. Here, the input parameters are the bow force F_b, velocity v_b and position along the string x_b, which may be time-varying. The output is given by the membrane displacement at the output location, as per (41).

4. TIME DISCRETISATION

Now, time is discretised with a time step k, yielding a sample rate $f_s = 1/k$. Then, a continuous function $u(t)$ is approximated at time step $t = nk$ by the time series u^n. Time difference operators are then introduced, as:

$$\delta_t^\pm u^n := \pm(u^{n\pm1} - u^n)/k, \;\; \delta_t^\circ u^n := (u^{n+1} - u^{n-1})/2k. \quad (43)$$

The second time difference is defined by combining the operators above: $\delta_t^2 u^n := \delta_t^+ \delta_t^- u^n$. Finally, a time averaging operator is defined as:

$$\mu_t^+ u^n := (u^{n+1} + u^n)/2. \quad (44)$$

4.1. String-Bridge System

It is now possible to adapt the numerical solver proposed in [7, 6] to numerically integrate equation (42a) in time. To that end, (42a) is first turned into a $2N_\mathrm{u} \times 2N_\mathrm{u}$ system of first-order-in-time equations. Thus, define $\mathfrak{q} := \mathbf{\Omega}_\mathrm{u}\mathfrak{u}$, $\mathfrak{p} := \dot{\mathfrak{u}}$. Therefore, (42a) becomes:

$$\begin{aligned} \begin{bmatrix} \dot{\mathfrak{q}} \\ \dot{\mathfrak{p}} \end{bmatrix} &= \underbrace{\begin{bmatrix} \mathbf{0} & \mathbf{\Omega}_\mathrm{u} \\ -\mathbf{\Omega}_\mathrm{u} & -\mathbf{\Omega}_\mathrm{u}^{-1}\mathbf{C}_u \end{bmatrix}}_{\mathbf{G}} \begin{bmatrix} \mathfrak{q} \\ \mathfrak{p} \end{bmatrix} - \begin{bmatrix} \mathbf{0} \\ \mathbf{\Omega}_\mathrm{u}^{-1}\boldsymbol{\xi}_\mathrm{b} \end{bmatrix} F_\mathrm{b}\phi(\eta), \\ \eta &= \left[\mathbf{0}, \boldsymbol{\xi}_\eta^\intercal\right] \begin{bmatrix} \mathfrak{q} \\ \mathfrak{p} \end{bmatrix} - v_\mathrm{b}. \end{aligned} \quad (45)$$

A second-order accurate, non-iterative numerical scheme is given as:

$$\boldsymbol{\sigma}^n \begin{bmatrix} \delta_t^+ \mathfrak{q}^n \\ \delta_t^+ \mathfrak{p}^n \end{bmatrix} = \mathbf{G} \begin{bmatrix} \mu_t^+ \mathfrak{q}^n \\ \mu_t^+ \mathfrak{p}^n \end{bmatrix} - \begin{bmatrix} \mathbf{0} \\ \mathbf{\Omega}_\mathrm{u}^{-1}\boldsymbol{\xi}_\mathrm{b} \end{bmatrix} F_\mathrm{b} \frac{\phi(\eta^n)}{\eta^n} \mu_{t+}\eta^n. \quad (46)$$

The form of $\boldsymbol{\sigma}^n$, adapted from [6], is:

$$\boldsymbol{\sigma}^n = \mathbf{I} + \frac{kF_\mathrm{b}}{2} \left(\frac{d\phi}{d\eta} - \frac{\phi}{\eta} \right)_{t=kn} \begin{bmatrix} \mathbf{0} \\ \mathbf{\Omega}_\mathrm{u}^{-1}\boldsymbol{\xi}_\mathrm{b} \end{bmatrix} \left[\mathbf{0}, \boldsymbol{\xi}_\eta^\intercal\right], \quad (47)$$

and is well-defined, owing to (2). Here, $\mathbf{J}_\mathrm{b}$ and $\mathbf{U}$ are as per Section 3.1.1 and 3.1.2, respectively. Expanding out the operators in (46), one is able to compute $\mathfrak{q}^{n+1}$, $\mathfrak{p}^{n+1}$ as the solution of a single linear system, thus avoiding entirely the need for iterative nonlinear root finders. The update equation in this case is:

$$\left(\mathbf{I} + \frac{kF_\mathrm{b}}{2} \left(\frac{d\phi}{d\eta} \right) \begin{bmatrix} \mathbf{0} \\ \mathbf{\Omega}_\mathrm{u}^{-1}\boldsymbol{\xi}_\mathrm{b} \end{bmatrix} \left[\mathbf{0}, \boldsymbol{\xi}_\eta^\intercal\right] - \frac{k}{2}\mathbf{G} \right) \begin{bmatrix} \mathfrak{q}^{n+1} \\ \mathfrak{p}^{n+1} \end{bmatrix} = \mathbf{b}^n,$$

where $\mathbf{b}^n$ is known from previous time steps. It is seen that the update matrix is in the form of a block matrix with fully diagonal blocks, plus a rank-1 perturbation. This can be solved efficiently, via the Sherman-Morrison formula [21], as detailed in [6].

Stability of scheme (46) is somewhat harder to prove, though partial results are available in [7]. Provided one chooses a number N_u of modes lower than the Nyquist limit, empirical evidence suggests that the proposed scheme greatly outperforms simpler explicit designs such as forward Euler or Runge-Kutta-type algorithms [22] in terms of stability, while keeping compute times within reference bounds for efficient simulation.

4.2. Spring & Membrane

The numerical integration of (42b), (42c) may be performed simply as:

$$\delta_t^2 \mathfrak{v}^n = -\mathbf{\Omega}_\mathfrak{v}^2 \mathfrak{v}^n - \mathbf{C}_\mathfrak{v} \delta_t^\circ \mathfrak{v}^n + \boldsymbol{\xi}_\mathrm{p} F_\mathrm{p}^n, \quad (48a)$$

$$\delta_t^2 \mathfrak{w}^n = -\mathbf{\Omega}_\mathfrak{w}^2 \mathfrak{w}^n - \mathbf{C}_\mathfrak{w} \delta_t^\circ \mathfrak{w}^n + \boldsymbol{\xi}_c F_c^n. \quad (48b)$$

Various other designs are possible, varying greatly in terms of stability and spectral accuracy. An attractive alternative is represented by exact integrators [23, 2], though the schemes above yield a perceptually reasonable reverberation characteristic [8]. Note that stability conditions arise as: $\mathbf{\Omega}_{\mathfrak{v},\mathfrak{w}} < 2/k$. These set upper limits for the modal frequencies.

5. OUTPUT SIGNALS

Figure 8 displays the spectrograms of the normalised signals extracted from the three subsystems. The string physical values were the ones of a C2 cello string, taken from [14], while the bridge parameters were the same listed in Figure 5. The bow pressure was $F_\mathrm{b} = 0.02$ N, and the input and output positions were set to $0.73 \cdot L_\mathrm{s}$ and $0.34 \cdot L_\mathrm{p}$ respectively. The latter values were chosen empirically to obtain a Helmholtz motion-shaped output sound [2, Chapter 7]. The damping profile applied was the one proposed by Valette [24]. The spring parameters were the ones detailed in Figure 7. Finally, the membrane physical values were: $L_m = 0.5$ m, $T_m = 3000$ N m^{-1} and $\rho_m = 1.26$ Kg m^{-2}, and the output point was $(X_\mathrm{o}, Y_\mathrm{o}) = (0.47, 0.62) \cdot L_m$. A damping profile was chosen, for the spring and the membrane, which consists of a frequency-independent (F-I) and a frequency-dependent (F-D) part; as proposed by Bilbao [2, Chapter 7] the latter depends on the square of the mode number. The damping coefficients for the spring were taken from [18]; in the mebrane case, the F-I coefficient was set to 10, while the F-D one to 5×10^{-5}, both chosen empirically. Only a few seconds-long portion of data was analysed, in order to avoid including too many signal variations. The spring and the membrane act here as reverberant components. Panel (b) from Figure 8 clearly exhibits cross stripes which correspond to the spring chirps. The membrane, on the other hand, introduces a broadband signal, which mimics late reflections. This is clearly visible in Panel (c) from Figure 8. Sound samples can be found at the following Github link[3].

6. CONCLUSION

This paper presented a physical model of the yaybahar in the modal domain. To this end, a modal decomposition of its subcomponents was offered, including a model for the coupling between a vibrating string and a distributed bridge, and the analytic modal expansion of a helical spring. In addition, an energy-consistent method for connecting the instrument components was here presented, making use of boundary forces.

This work focused on the development of a yaybahar physical model; nevertheless, different aspects were overlooked, and will be

[3] https://github.com/Nemus-Project/yaybahar-nit

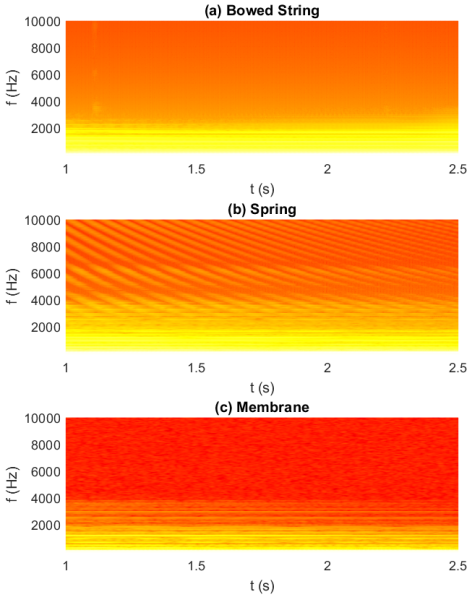

Figure 8: *Spectrograms of the three subsystems outputs after the initial transient. Panel (a) displays the spectrogram of the extracted force F_p, panel (b) shows the spectrogram of the force signal F_c, and panel (c) represents the output signal $\dot{w}_\mathrm{o}$ at the output position $(X_\mathrm{o}, Y_\mathrm{o})$.*

subject of future work. The physical values for the spring and the membrane were empirically tuned, while running proper measurements on a real instrument would significantly improve the sound quality. This is valid for the damping profiles as well. In addition, the membrane was considered to be rectangular, while an accurate reproduction would employ a circular model. Further future work will also include a real-time implementation.

7. ACKNOWLEDGMENTS

This work was supported by the European Research Council (ERC), under grant 2020-StG-950084-NEMUS.

8. REFERENCES

[1] J Parker and S. Bilbao, "Spring reverberation: A physical perspective," in *Proc. Digital Audio Effects (DAFx-09)*, Como, Italy, 09 2009.

[2] S. Bilbao, *Numerical Sound Synthesis*, John Wiley & Sons, Ltd, Chichester, UK, 2009.

[3] S. Bilbao, "Numerical simulation of spring reverberation," in *Proc. Digital Audio Effects (DAFx-13)*, Maynooth, Ireland, 09 2013.

[4] P.J. Christensen, S. Willemsen, and S. Serafin, "Applied Physical Modeling for Sound Synthesis: the Yaybahar," in *Proc. 2nd Nordic SMC Conf.*, Online, 11 2021.

[5] J. Parker, H. Penttinen, S. Bilbao, and J.S. Abel, "Modeling methods for the highly dispersive slinky spring: A novel musical toy," in *Proc. Digital Audio Effects (DAFx-10)*, Graz, Austria, 09 2010.

[6] Riccardo Russo, Michele Ducceschi, and Stefan Bilbao, "Efficient simulation of the bowed string in modal form," in *Proc. Digital Audio Effects (DAFx-2022), Vienna*, 09 2022.

[7] M. Ducceschi and S. Bilbao, "Non-iterative simulation methods for virtual analog modelling," *IEEE/ACM Trans. Audio Speech Lang. Process.*, vol. 30, pp. 3189–3198, 2022.

[8] M. Ducceschi and C.J. Webb, "Plate reverberation: Towards the development of a real-time plug-in for the working musician," in *Proc. Int. Conf. Acoust. (ICA 2016)*, Buenos Aires, Argentina, 09 2016.

[9] R. Russo, "Physical modeling and optimisation of a emt 140 plate reverb," M.S. thesis, Aalborg University Copenhagen, Copenhagen, Denmark, 2021.

[10] J.O. Smith, *Physical Audio Signal Processing*, `https://ccrma.stanford.edu/~jos/pasp/pasp.html`, accessed April 2023, online book, 2010 edition.

[11] J. Woodhouse, "On the "bridge hill" of the violin," *Acta Acust. united Acust.*, vol. 91, pp. 155–165, 2005.

[12] J.H. Smith and J. Woodhouse, "The tribology of rosin," *J. Mech. Phys. Solids*, vol. 48, pp. 1633–1681, 08 2000.

[13] P. Galluzzo, J. Woodhouse, and H. Mansour, "Assessing friction laws for simulating bowed-string motion," *Acta Acust. united Acust.*, vol. 103, pp. 1080–1099, 11 2017.

[14] C. Desvages, *Physical modelling of the bowed string and applications to sound synthesis*, Ph.D. thesis, The University of Edinburgh, 2018.

[15] W.H. Wittrick, "On elastic wave propagation in helical springs," *Int. J. Mech. Sci.*, vol. 8, no. 1, pp. 25–47, 1966.

[16] L. Della Pietra and S. della Valle, "On the dynamic behaviour of axially excited helical springs," *Meccanica*, vol. 17, pp. 31–43, 1982.

[17] J.N. Franklin, *Matrix Theory*, Dover Publications, Mineola, NY, USA, 2000.

[18] M. Van Walstijn, "Numerical calculation of modal spring reverb parameters," in *Proc. Digital Audio Effects (DAFx-2020), Online*, 09 2020.

[19] J. McQuillan and M. Van Walstijn, "Modal spring reverb based on discretisation of the thin helical spring model," in *Proc. Digital Audio Effects (DAFx-2021), Online*, 09 2021, vol. 2.

[20] L.E. Kinsler, A.R. Frey, A.B. Coppens, and J.V. Sanders, *Fundamentals of Acoustics, 4th Edition*, Wiley, Hoboken, NJ, USA, 1999.

[21] J. Sherman and W.J. Morrison, "Adjustment of an inverse matrix corresponding to a change in one element of a given matrix," *Ann. Math. Stat.*, vol. 21, pp. 124–127, 1950.

[22] R.J. LeVeque, *Finite Difference Methods for Ordinary and Partial Differential Equations. Steady State and Time Dependent Problems*, SIAM, Philadelphia, USA, 2007.

[23] J. Cieslinski, "On the exact discretization of the classical harmonic oscillator equation," *J. Differ. Equ. Appl.*, vol. 17, no. 11, pp. 1673–1694, 2009.

[24] C. Valette and C. Cuesta, *Mécanique de la corde vibrante*, Hermès, Paris, 1993.